Mechanical Robustness of Graphene on Flexible Transparent Substrates

Moon H. Kang,*,[†] Lizbeth O. Prieto López,[‡,§] Bingan Chen,[‖] Ken Teo,[‖] John A. Williams,[§] William I. Milne,[†,‖] and Matthew T. Cole*,[†]

[†]Electrical Engineering Division, Department of Engineering, University of Cambridge, 9 J. J. Thomson Avenue, Cambridge CB3 0FA, United Kingdom

[‡]INM-Leibniz Institute for New Materials, Campus D2 2, 66123 Saarbruecken, Germany

[§]Mechanics, Materials & Design Division, Department of Engineering, University of Cambridge, Trumpington Street, Cambridge CB2 1PZ, United Kingdom

[‖]Aixtron, Buckingham Business Park, Swavesey CB24 4FQ, United Kingdom

[⊥]Quantum Nanoelectronics Research Center, Tokyo Institute of Technology, Tokyo 152-8550, Japan
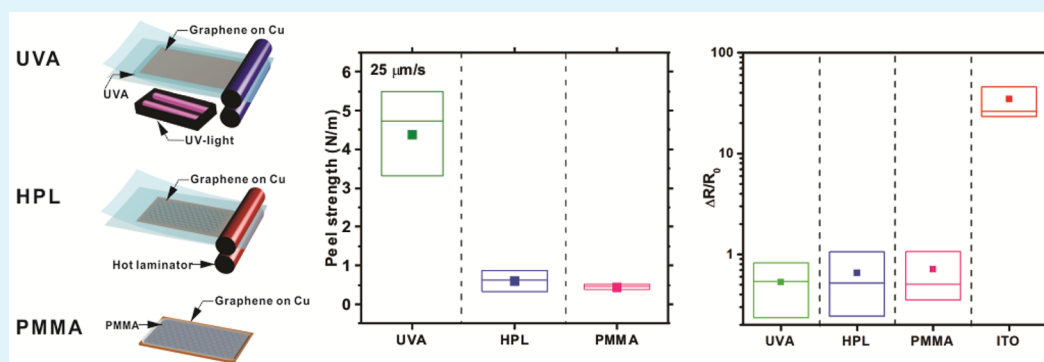
ABSTRACT: This study reports on a facile and widely applicable method of transferring chemical vapor deposited (CVD) graphene uniformly onto optically transparent and mechanically flexible substrates using commercially available, low-cost ultraviolet adhesive (UVA) and hot-press lamination (HPL). We report on the adhesion potential between the graphene and the substrate, and we compare these findings with those of the more commonly used cast polymer handler transfer processes. Graphene transferred with the two proposed methods showed lower surface energy and displayed a higher degree of adhesion (UVA: 4.40 ± 1.09 N/m, HPL: 0.60 ± 0.26 N/m) compared to equivalent CVD-graphene transferred using conventional poly(methyl methacrylate) (PMMA: 0.44 ± 0.06 N/m). The mechanical robustness of the transferred graphene was investigated by measuring the differential resistance as a function of bend angle and repeated bend−relax cycles across a range of bend radii. At a bend angle of 100° and a 2.5 mm bend radius, for both transfer techniques, the normalized resistance of graphene transferred on polyethylene terephthalate (PET) was around 80 times less than that of indium−tin oxide on PET. After 10^4 bend cycles, the resistance of the transferred graphene on PET using UVA and HPL was found to be, on average, around 25.5 and 8.1% higher than that of PMMA-transferred graphene, indicating that UVA- and HPL-transferred graphene are more strongly adhered compared to PMMA-transferred graphene. The robustness, in terms of maintained electrical performance upon mechanical fatigue, of the transferred graphene was around 60 times improved over ITO/PET upon many thousands of repeated bending stress cycles. On the basis of present production methods, the development of the next-generation of highly conformal, diverse form factor electronics, exploiting the emerging family of two-dimensional materials, necessitates the development of simple, low-cost, and mechanically robust transfer processes; the developed UVA and HPL approaches show significant potential and allow for large-area-compatible, near-room temperature transfer of graphene onto a diverse range of polymeric supports.

KEYWORDS: CVD graphene, flexible electronics, surface energy, optical transparency, large-area transfer, time stability, adhesion

INTRODUCTION

The ever increasing demands on functionality from consumer electronics has highlighted the need for a wider class of mechanically flexible transparent conductors. Graphene, a two-dimensional, hexagonally latticed graphitic carbon allotrope has been demonstrated as a near-perfect transparent conductor.[1,2] It is widely anticipated that graphene will complement indium and fluorine tin oxide (ITO/FTO) in large-area transparent electronics, in applications such as organic light-emitting diodes

(OLED),[3−6] touch screens,[7,8] and photovoltaic cells.[9−11] Metal oxide thin films, such as ITO, FTO, and Al-doped ZnO, though widely adopted are inherently brittle,[12] while metallic serpentines and ultrathin Si, though mechanically flexible, add optically undesirable features, such as image blurring and a broad reduction in transparency. Similarly, organic solution-cast alternatives, such as PEDOT:PSS, though extremely flexible often have undesirable characteristic hues. The high conductivity, high flat broadband optical transparency, and impressive mechanical flexibility of graphene make it one of the leading materials for the development of novel plastic electronics.

Though there have certainly been many reported micro- and nanoelectronics devices fabricated using chemically and mechanically exfoliated graphene inks, such devices lack a truly layered structure, with the resulting films formed from highly disordered graphene flakes. Such a lack of short-range order smears the nascent mechano-optoelectronic properties of the graphene on which they are fabricated.[13−16] These percolative networks are often formed from graphene flakes that are a few micrometers in size and are not contiguous, limiting their practicality and micrometer-scale uniformity.[17−21] CVD has therefore come to the fore as one of the few commercially viable approaches, offering cost savings and the potential for true monolayer graphene devices on very large area substrates with large grains and high yields.[22−27] Indeed, if graphene devices on flexible substrates are to be realized, then given the present production limitations, large-area-compatible single-layer transfer techniques that retain the graphene's layered planar structure must be developed, alongside methods to grow directly on technologically useful substrates. Little progress has been made in the latter given the prohibitively low thermal budgets associated with such substrates and the associated reduction in

the graphene quality;[28−30] however, much scope exists for the development of novel transfer methods that employ high-quality CVD graphene.

Although the optical and electrical continuity of CVD graphene shows much merit, the primary limitation preventing the wider-scale adoption of CVD-based graphene technologies is that it must be transferred to arbitrary substrates from the opaque conducting catalyst on which it was grown. The transfer method is crucial in realizing useful devices; it intimately dictates the final conductivity and optical transparency. Soft transfer processes must be developed as the native quality of CVD graphene can be readily deteriorated through aggressive transfer processes. Perhaps the most commonly employed transfer method to date is that where the graphene is supported by a polymer handler, such as poly(methyl methacrylate) (PMMA) or polydimethylsiloxane (PDMS), while the catalyst is chemically etched.[17−21] This polymer-supported graphene is subsequently placed on an arbitrary substrate and the polymer handler removed in a solvent bath.[17−21] PMMA transfer requires skilled users, is costly, has low throughput and low yields, and is not compatible with large-area electronics in a mass-production context. In 2010, Bae et al., for the first time, in a viable roll-to-roll process, transferred large-area CVD graphene onto plastic.[6] In that study, CVD graphene was attached to thermal-release tape using a roll-to-roll system, and the tape was removed following the graphene transfer by heating to 100 °C.[6] This transfer method did not leave significant residues and made graphene transfer on large scales possible. Despite its advantages, graphene adhesion to the plastic substrates remains a critical issue in assessing the technological merit of such graphene-based devices. Should the adhesion prove to be weak in such systems, since the transferred graphene is physically adsorbed without strong
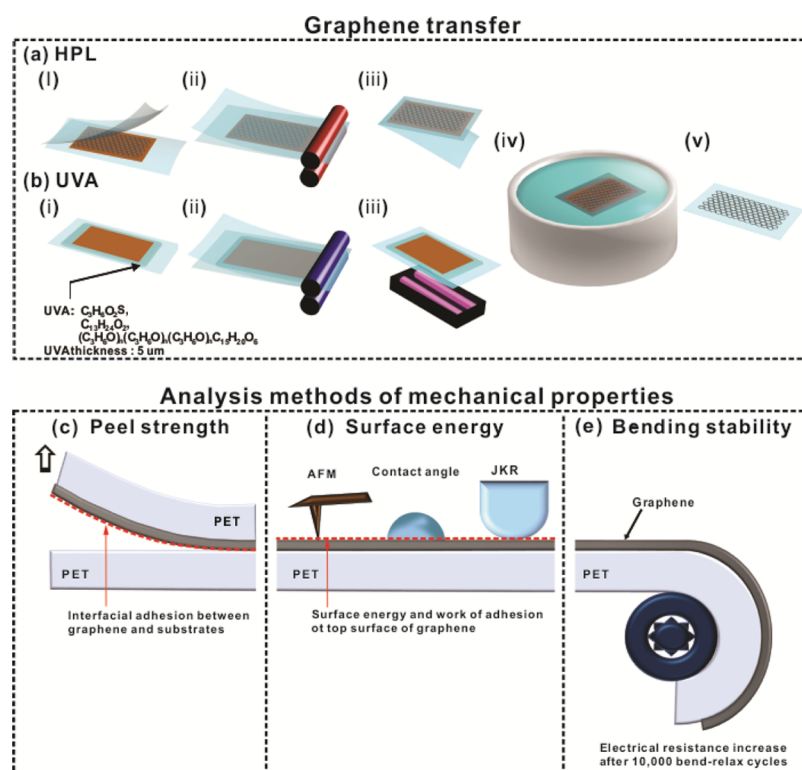
Figure 1. Schematic depiction of graphene transfer using (a) hot-press lamination (HPL) and (b) UV adhesive (UVA). Analysis methods of mechanical properties of graphene on a PET substrate: (c) interfacial adhesion between graphene and the substrate, (d) surface energy of top surface of graphene, and (e) bending stability of graphene after 10^4 bending cycles.

adhesion between the substrate and graphene, then flexible electronic devices based on such materials and processes will be of little commercial value as the graphene would readily delaminate. Weak interfacial adhesion remains a critical barrier in realizing a stable polymer-transfer process for robust graphene-based thin film electronics.

In the present study we propose two alternative transfer techniques, hot-press lamination (HPL) transfer and ultraviolet adhesive (UVA), which form strong adhesion between the graphene and substrate.[31] Both of the proposed methods ensure mechanically stable graphene transfer with strong and long-lasting adhesion. We analyze the mechanical properties of the graphene attached to flexible substrates using both approaches and compare this to conventional PMMA-mediated transfer. The mechanical and electrical stability of the UVA and HPL approaches are considered, as are the surface energy, adhesion potential, and bending stress stability.

■ UVA AND HPL GRAPHENE TRANSFER

Graphene was grown, as reported in Kang et al.,[31] using a commercially available Aixtron Black Magic Pro, hot-walled thermal CVD system on 25 μm Cu foil (99.999% Alfa Aesar) under 5 sccm CH_4 (99.5%) at 1000 °C in Ar/H_2 (960 (99.9997%)/40 (99.9992%) sccm) at 25 mbar. Following 15 min of growth, samples were quenched under 2000 sccm N_2 (99.99%) to 250 °C and removed from the reactor. Graphene grains were approximately 10−100 μm in diameter with a mean area of 400 μm^2. From SEM and Raman spectroscopy, we find that the as-synthesized polycrystalline graphene coalesced to form large-area, few-layer graphene thin films with a nominal layer count of 1−2.

Figure 1a,b depicts the HPL and UVA transfer methods, respectively. For HPL, the graphene-on-catalyst was attached to commercially available thermally activated ethylene vinyl acetate (EVA)-treated PET substrates (GBC Co.). As illustrated in Figure 1a, first the as-synthesized graphene-on-catalyst was sandwiched between two EVA-PET substrates (i), and then passed through a dual roller laminator heated to 120 °C (ii). The backside EVA-PET was detached (iii), with the conformal graphene coating on this side being removed in the process. The now-exposed Cu was then etched in $(NH_4)_2S_2O_8$ in deionized (DI) water (1 M) for 12 h (iv). The PET-supported graphene samples were then rinsed with DI water and gently blow-dried in ultrahigh purity N_2 (v). The transfer process is substrate-invariant. It can be applied to a wide variety of polymeric substrates whose glass transition temperature is greater than the roller temperature. In the UV-assisted adhesive method, to chemically adhere the graphene we employ a UV-cured adhesive (Norland Co.), consisting of methyl thioglycoate ($C_3H_6O_2S$), isodecyl acrylate ($C_{13}H_{24}O_2$), and trimethylolpropane polypropylene glycol triacrylate ($(C_3H_6O)_n(C_3H_6O)_n(C_3H_6O)_nC_{15}H_{20}O_6$). As illustrated in Figure 1b, UVA was first coated onto the polymer substrate, and the as-grown graphene-on-catalyst was placed in contact with the cast UVA (i). The sandwich was then compressed at 0.2 MPa using a cold-roll laminator, ensuring that all air pockets were removed to maximize the interface adhesion (ii). The UVA adhesive was cured by exposing the PET backside to a UV optical source (365 nm, 22 mW/m^2) for 15 min (iii). Following UV curing, the Cu foil was etched in aqueous $(NH_4)_2S_2O_8$ for 12 h (iv), then rinsed in DI water and dried in high-purity N_2 as before (v). Note that all UVA processing was undertaken at room temperature, making the approach applicable to a wide range of polymer substrates.

In the case of conventional PMMA transfer, a thin layer (ca. 100 nm) of PMMA is first cast on the graphene-on-catalyst, where the catalyst is subsequently wet-etched in its entirety with the graphene/PMMA bilayer floated on the etchant solution. The bilayer is then manually scooped from the aqueous etchant surface and transferred to an arbitrary substrate in a process which requires highly trained individuals or precisely controlled machinery. After scooping, the transferred graphene is then dried in air for >12 h. The PMMA support is then removed via thermal or additional aqueous treatments. Adoption of our HPL and UVA approaches makes many of these process-intensive steps redundant. As a result, we estimate from our optimized processing an increase in yield of up to 10% compared to that of conventional PMMA transfer, coupled to an increased throughput due to the decrease in total processing time.

In both cases, the as-grown graphene-on-catalyst achieves intimate contact with the EVA melt and to the low-viscosity UVA prior to curing. To attain a robust mechanical interface, the graphene requires proximal contact to the substrate.[32] The two transfer methods described above allow for robust adhesion via processes that are simple, fast, applicable to a wide range of substrates, high-yield, and large-area-compatible at a low-cost per unit area. Over many thousands of cycles, our experiments have shown that the outlined adhesion strategies provide strong and long-lasting adhesion between the as-synthesized graphene and the flexible transparent substrates. We stress here that throughout we employ a highly calibrated, large-area (>100 cm^2) CVD graphene growth protocol in order to provide repeatable source graphene. To confirm sample-to-sample uniformity, we independently verified the as-grown graphene via multiple point and mapping Raman spectroscopy to ensure equivalent source materials prior to transfer.

■ ROBUST MECHANICAL ADHESION

Graphene is intrinsically mechanically flexible.[33,34] Unlike the various alternative transparent conducting oxides, graphene does not readily suffer microcrack formation when strained. Rather, mobile grain boundaries and inter- and intralattice strain accommodate large mechanical deformations with a maximum failure strain of up to 15−20%,[35] making graphene particularly well-suited to future flexible transparent electronic devices. Recent advances in large-area CVD graphene synthesis have shown high-area uniformity across materials that maintain their polycrystalline macrostructure and that are contiguous over large areas when compared to mechanically exfoliated graphene inks. As illustrated in Figure 1c−e, to confirm the functionality of the UVA and HPL transfer methods outlined above, we have analyzed three critical mechanical properties of the transferred graphene on PET substrates, namely, the interfacial adhesion between the graphene and the substrate (Figure 1c), the surface energy of the uppermost graphene surface (Figure 1d), and the bending fatigue stability (Figure 1e).

The magnitude of the peel force per unit width (F_a) is a measure of the strength of the bonds between the PET substrate, the adhesive, and the graphene layer. Conversely, the effective surface energy (γ), or work of adhesion (W_{12}), provides a measure of the graphene coverage and the degree of defect induction as a result of the transfer process.[36−40]

The surface energy is a measure of the disruption of intermolecular bonds that occurs when a surface is created. It can be defined as the reversible work required to create a unit area of surface from a bulk material. In the case of a brittle material, the work of adhesion required to generate a unit area of separation
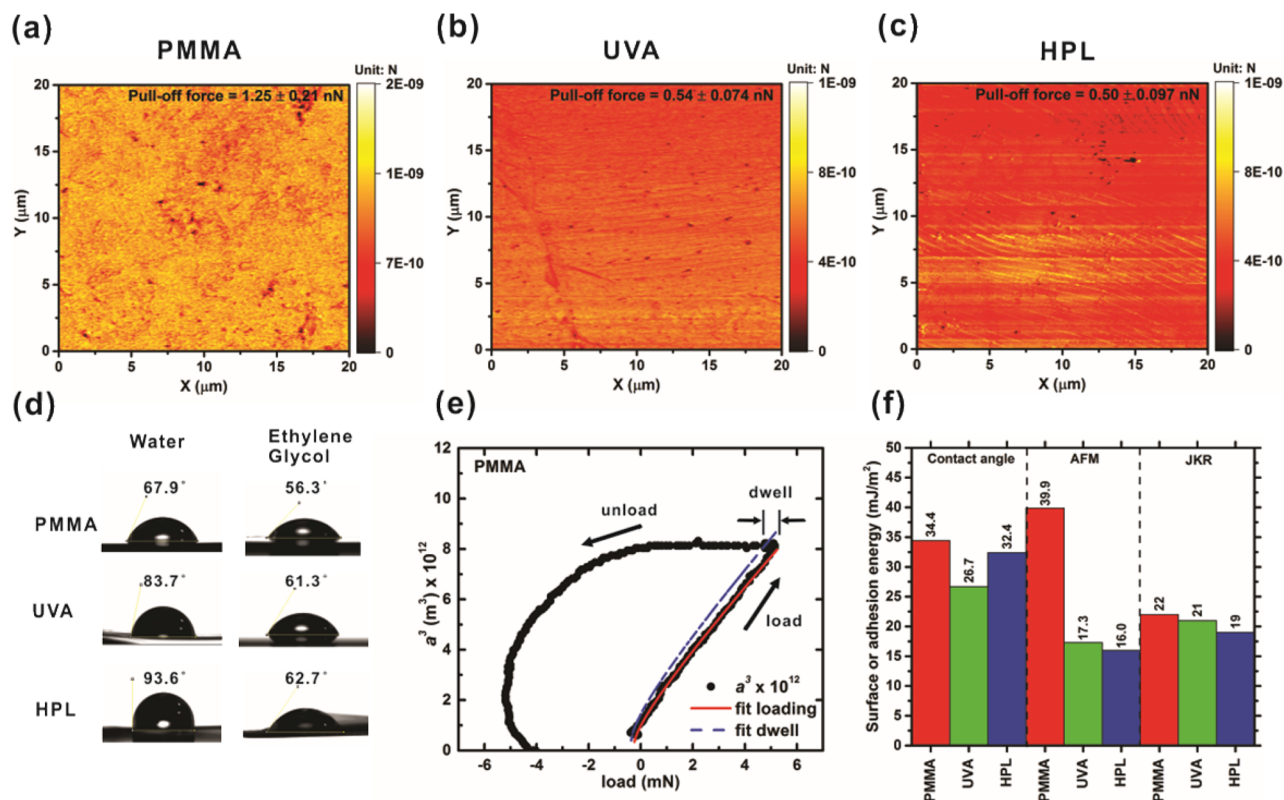
Figure 2. AFM pull-off forces for (a) PMMA-, (b) UVA-, and (c) HPL-transferred graphene. (d) Variation in contact angle as a function of transfer method. (e) Typical JKR load−contact area response. (f) Summary of the surface energies and work of adhesion from contact angle, AFM, and JKR measurements.

will be equal to 2γ. When a stress plane separates two disparate materials, the theoretical work of adhesion can be thermodynamically defined as W_{12}[41] and is given by

$$W_{12} = \gamma_{S1} + \gamma_{S2} - \gamma_{12} \tag{1}$$

where subscripts S1 and S2 refer to the two materials and subscript refers 12 to the interface between them. If purely dispersive forces, as opposed to polar, are responsible for the interaction between materials 1 and 2, then[41]

$$W_{12} = 2\sqrt{\gamma_{S1}\gamma_{S2}} \tag{2}$$

The work of adhesion can then be estimated by measuring the pull-off force of a scanning AFM tip. Experimental values of the pull-off force account not only for interfacial bond rupture, i.e., W_{12}, but also any viscoelastic energy dissipation at the advancing crack tip. Thus, in many cases, the measured work of adhesion W_{ad} will be greater than W_{12}. Measures of W_{12} thus place a lower bound on the work of adhesion W_{ad}.

The most common technique to assess surface energy γ_S is via contact angle (θ) assessment with two or more standard liquid probes. The relationship between the surface energy and θ is given by the Young−Dupré equation[42]

$$\gamma_S = \gamma_{SL} + \gamma_L \cos\theta \tag{3}$$

where γ_L and γ_S are the surface energies of the liquid and solid, respectively, and γ_{SL} is the surface energy of the solid−liquid interface. On the basis of the Owens−Wendt model,[43] γ_{SL} can be estimated from

$$\gamma_{SL} = \gamma_S + \gamma_L - 2(\gamma_S^d\gamma_L^d)^{1/2} - 2(\gamma_S^p\gamma_L^p)^{1/2} \tag{4}$$

in which the superscipts d and p refer to the dispersion and polar contributions to surface energy, such that

$$\gamma_S = \gamma_S^d + \gamma_S^p \quad \text{and} \quad \gamma_L = \gamma_L^d + \gamma_L^p \tag{5}$$

Substituting eq 4 into eq 3, we obtain

$$\gamma_L(1 + \cos\theta) = 2(\gamma_S^d\gamma_L^d)^{1/2} + 2(\gamma_S^p\gamma_L^p)^{1/2} \tag{6}$$

Thus, using two liquid probes with known γ_L^d and γ_L^p and two experimental values of θ, we can solve for γ_S^d and γ_S^p and hence evaluate γ_S. At room temperature and ambient pressure, the surface energies of water and ethylene glycol are 72.8 mJ m^{-2} ($\gamma_L^d + \gamma_L^p = 24.7 + 48.1$) and 48.3 mJ m^{-2} ($\gamma_L^d + \gamma_L^p = 30.9 + 17.4$), respectively.[44] Contact angles were measured using an optical contact system (CAM200, LOT-Oriel, Ltd.) and are shown in Figure 2d. The calculated surface energies are shown in Figure 2f. The UVA and HPL transfers showed somewhat lower surface energies (26.7 and 32.4 mJ m^{-2}, respectively) compared to that of the PMMA-transferred graphene (34.4 mJ m^{-2}).

In principle, direct measurements of adhesion can be carried out by loading a spherical indenter into contact with the surface and then measuring the tensile load required to break the adhesive contact. If both surfaces are rigid, then the pull-off force P_a is given by the Bradley equation[45]

$$P_a = 2\pi R W_{ad} \tag{7}$$

and W_{ad} will be equal to W_{12}. When the surfaces show a linear elastic behavior, a finite circular contact spot will be generated during the compressive loading stage. In the absence of any energetic interactions, its radius a is given by the Hertz relation between compressive load F and the system elastic constant K.

$$a_H^3 = \frac{RF}{K} \quad \text{where} \quad \frac{1}{K} = \frac{3}{4}\left\{\frac{1-\nu_1^2}{E_1} + \frac{1-\nu_2^2}{E_2}\right\} \tag{8}$$

Here, E is the Young's modulus and ν is the Poisson's ratio. In the presence of adhesive effects, the value of a will be enhanced, and provided both surfaces are of high moduli (as is the case in atomic force microscopy), it can be described by the relation often attributed to DMT[44]

$$a_{DMT}^3 = \frac{R}{K}\{F + 2\pi RW_{12}\} \tag{9}$$

In this case the magnitude of the pull-off force P_a remains as given by eq 7. The adhesion force in a 20 μm × 20 μm area was scanned via AFM (Bruker's Dimension Icon). Figure 2a−c shows maps of the measured pull-off force from graphene transferred onto PET substrates by PMMA, UVA, and HPL, respectively. PMMA-transferred graphene has the highest adhesion (1.25 nN) with the largest standard deviation (±0.21 nN), highlighting its lack of spatial uniformity, while UVA (0.54 ± 0.074 nN) and HPL (0.502 ± 0.097 nN) showed similar values to one another, both some 58% lower than PMMA. We also note the lower standard deviation associated with these spatially uniform transfer methods, suggesting improved spatial uniformity in the transfer process. Conversion of the pull-off force P_a to the work of adhesion W_{ad} assumes that the tip has a spherical profile of known radius R. If the value of the tip radius is taken to be 5 nm, then W_{ad} can be evaluated from eq 7, and the graphene surface energy (γ_g) can in turn be estimated using eq 2[46] as

$$\gamma_g = W_{ad}^2/4\gamma_p \tag{10}$$

where γ_p is the surface energy of silicon probe, taken to be 55.6 mJ m^{-2}.[47] Information on the adhesion of soft macroscopic systems (0.1−5.0 mm) can be obtained from adhesion tests based on JKR analysis.[48] Here, adhesion between a soft polymer sphere and the graphene surface is probed. Again, during compressive loading the radius of the contact spot will be larger than in a simple Hertz case. However, in this case the detailed value depends critically on the work of adhesion, the probe radius R, the surface stiffness K, and the applied compressive force F, as given by

$$a_{JKR}^3 = \frac{R}{K}\left(F + 3\pi W_{12}R + \sqrt{6\pi W_{12}RF + (3\pi W_{12}R)^2}\right) \tag{11}$$

The indenter used in this study was a PDMS hemisphere of radius 3.51 mm with Young's modulus $E = 2.6$ MPa and Poisson's ratio $\nu = 0.49$. The loading program had a preload of 5 mN, a dwell period of 60 s, and a loading/unloading speed of 0.1 μm/s. In a JKR test, the pull-off load is given by the relation

$$P_a = \frac{3\pi}{2}RW_{ad} \tag{12}$$

The soft polymer surface is capable of absorbing significant mechanical energy through its viscoelastic behavior, so measured values of W_{ad} are inevitably much greater than W_{12} and are influenced by the speed of the detachment.[49] The rig used in the study enabled independent measurements to be made of both the contact force and optically of the contact area. A representative plot of force versus contact spot dimension, plotted as a^3 is shown in Figure 2f. Rearrangement of eq 11

provides an expression for W_{ad} in terms of the load P and spot size a.

$$W_{ad} = \frac{1}{6\pi a^3}\left(\frac{a^3K}{R} - P\right)^2 \tag{13}$$

By curve fitting eq 13 to the loading stage of the test, it is possible to find an empirical value of the effective stiffness K and compare this with the value given from independent measurements of the polymer properties E and ν. In practice, the layer of adhesive immediately below the graphene introduces an element of compliance into the system, thus marginally reducing the combined surface stiffness K. Similarly, fitting eq 13 to the observed value of the cube of the contact area radius at the end of the dwell period allowed an estimate to be made of W_{ad} under quasi-steady-state conditions. Although the nominal speed of detachment speed was kept constant at 100 nm s^{-1} during the unloading process, the rate at which the radius of the contact spot decreases as it recedes, and this is reflected in a significant and growing increase in the effective value of W_{ad}. Typically, against the surface examined this grew from around 20 mJ m^{-2} under steady conditions to more than 300 mJ m^{-2} at the point of detachment.

The measured values of work of adhesion of graphene transferred by the three methods (contact angle, AFM, and JKR indentation) are shown in Figure 2f. The work of adhesion between the graphene surface and probing material is strongly correlated to the morphology of the graphene surface and the number of layers as well as the area density of lattice defects.[36−40] Defective graphene is manifestly stickier. Lattice vacancies increase the polarity of the surface resulting in an increase in the surface energy and thus a lower bound in the work of adhesion.[37,39,40] If defect free graphene is perfectly transferred with no induced defects, then the resulting interface has a very low work of adhesion. Similarly, the more graphene layers that are stacked, the lower the work of adhesion.[36,39] However, graphene can be easily damaged during conventional transfer processes, which likely creates macroscopic defects.[50] If the substrate is not completely covered and the transferred material has a significant number of vacancies during the selected transfer process, then the work of adhesion increases. Though functionally beneficial for sensors and similar applications, should the transferred graphene have a coverage that is less than that defined by percolation theory, the resulting flexible transparent conductor will be of little use due to its prohibitively high sheet resistance. If a second and third layer of graphene is transferred, then there is a higher probability of covering said lattice vacancies in the first transfer. The higher values of the surface energy and work of adhesion of PMMA-transferred graphene and lower values of UVA- and HPL-transferred graphene suggests that the area coverage of graphene is likely higher in the UVA and HPL transfers than that for PMMA transfer.

To further investigate the degree of adhesion between the graphene and the substrate in each transfer case, T-peel tests were conducted. T-peel tests are a qualitative method primarily intended for determining the relative peel resistance of adhesive bonds between flexible adherents.[51] The T-peel strength is the average load per unit width of a bond line required to separate progressively a flexible member from another flexible member. Our T-peel test scheme is depicted in Figure 3a. The adherents have such dimensions and physical properties so as to permit bending them through any angle up to 90° without cracking. Failure follows a path of least resistance, which may be cohesive

E
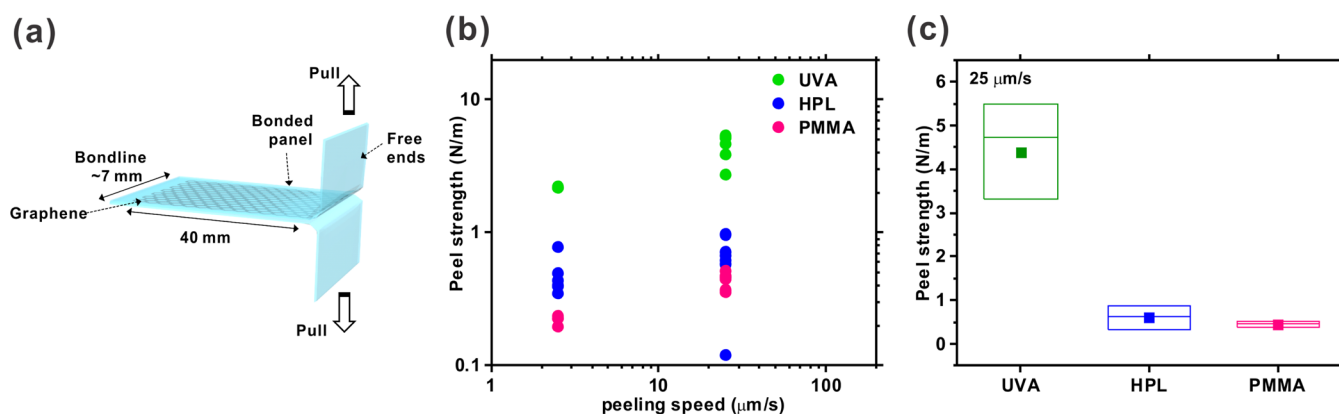
Figure 3. (a) T-peel test scheme. (b) Variation in peel strength as a function of peel speed. (c) Distribution in the peel strength across the considered transfer methods (25 μm/s peeling speed).

through one element of the structure or interfacial and so along the interface between two elements in the specimen.

In all the specimens, the graphene was sandwiched between two PET sheets and was attached to one of these using the UVA cured adhesive. The bond to the second sheet of PET was formed by either the UVA adhesive, the HPL melt, or the natural adhesion between the PMMA-transferred graphene. In this case the graphene−PET bond was established by floating the PMMA-graphene sample on water before transferring this onto the PET sheet and after drying removing the PMMA by treatment with acetone. Two peeling speeds were evaluated (2.5 and 25 μm/s). Specimens were 7 mm wide. Figure 3b shows the variation in peeling strength. A low peel strength represents weak adhesion between the elements of the laminate and substrate, while a high peel strength suggests that the graphene strongly adheres to its substrate. As summarized in Figure 3c, the UVA-transferred graphene laminate showed the highest peel strength (4.39 ± 1.09 N/m), followed by the HPL-transferred graphene structure (0.60 ± 0.26 N/m) and the PMMA-transferred graphene structure in which the bond between graphene and PET relied solely on the van der Waals forces, showing as anticipated the lowest (0.44 ± 0.06 N/m). The substrate adhesion strength of the UVA and HPL graphene are some 880 and 29% higher, respectively, than that of mechanically exfoliated graphene on SiO$_2$ (0.45 ± 0.02 N/m).[52] These results further demonstrate conclusively that UVA transfer allows for significantly enhanced adhesion between PET substrates and CVD graphene over the more conventionally used PMMA-based techniques. Thermal-release tape and other such transfer techniques will latterly be considered under the present experimental framework and reported elsewhere.

To assess the mechanical robustness of the transferred graphene, cyclic bending fatigue tests were conducted using a custom-built, LabVIEW-controlled bending stress system which measures the current−voltage (I−V) and automatically extracts the differential resistance at zero bias, $R = (dV/dI)_{V=0}$, following a controlled bend of defined angle for a defined bend radius (R_b). As shown in the inset of Figure 4a, the system mechanically statically clamps both ends of a specimen, where these clamps also serve as electrical probes connected to a Keithley 2600 source-measure unit. The conducting channel was 11 mm × 70 mm. The central backside section of the specimens were supported by changeable cylinders of well-defined bend radii. The robustness of graphene/PET transferred with our three transfer approaches (PMMA, UVA, and HPL) and ITO/PET was assessed with two types of

bending tests: bend angle variation and bending fatigue. For the bending fatigue tests, 10^4 bend−relax cycles were conducted and the differential resistance measured at the flat (0°) and bent (90°) positions after each cycle. For the bend angle experiments, a fixed R_b of 2.5 mm was used, and the bend angle increased from 0 to 100°, at 10° increments. The measured resistance as a function of bend angle is shown in Figure 4a. The differential resistance (herein denoted R) was measured at each bend angle and normalized with R_0 (the initial resistance measured at 0°). The three transferred graphene approaches showed negligible variation in resistance as a function of bend angle, whereas the resistance of ITO increased sharply at bend angles >40°. All the graphene samples demonstrated a low normalized resistance even at 100° (1.05, PMMA; 0.94, UVA; and 1.04, HPL), which is around 80 times less than that of ITO/PET (79.8). Certainly, the mechanical robustness of transferred graphene is, regardless of the transfer method employed, far superior to ITO.

Of the three graphene transfer approaches, we find that compared to conventional PMMA graphene UVA graphene exhibits lower resistance throughout all bending angles with HPL graphene showing a lower resistance at bend angles >40°. For both UVA and HPL samples, the normalized resistance did not tend to increase with bend angle, while it did for PMMA graphene. UVA and HPL graphene appear more robust than PMMA graphene in high-bend-angle applications, such as e-paper and wearable sensors. Bending strain is a known precursor for thin film delamination. If the degree of adhesion is lowered as a result of the PMMA transfer process employed, then in many cases this naturally manifests in a limited degree of motion such devices can accommodate. Indeed, bending readily encourages further delamination of already weakly adhered zones, thereby rapidly degrading over time and cycle number the sample's mechanical robustness.[50] CVD synthesis results in the formation of a polycrystalline two-dimensional material with low, yet still unavoidable, vacancies and line defects, both of which likely further form during the transfer process. Such defects tend to nucleate additional defects resulting in microcrack formation, particularly between grains where the graphene is otherwise weakly bound to the substrate. Contrary to conventional PMMA-transferred graphene, which is bound solely by van der Waals interactions, UVA and HPL graphene has herein evidenced firm binding. This enhanced adhesion mediates improved strain distribution resulting in reduced crack formation compared to that of PMMA graphene under equivalent
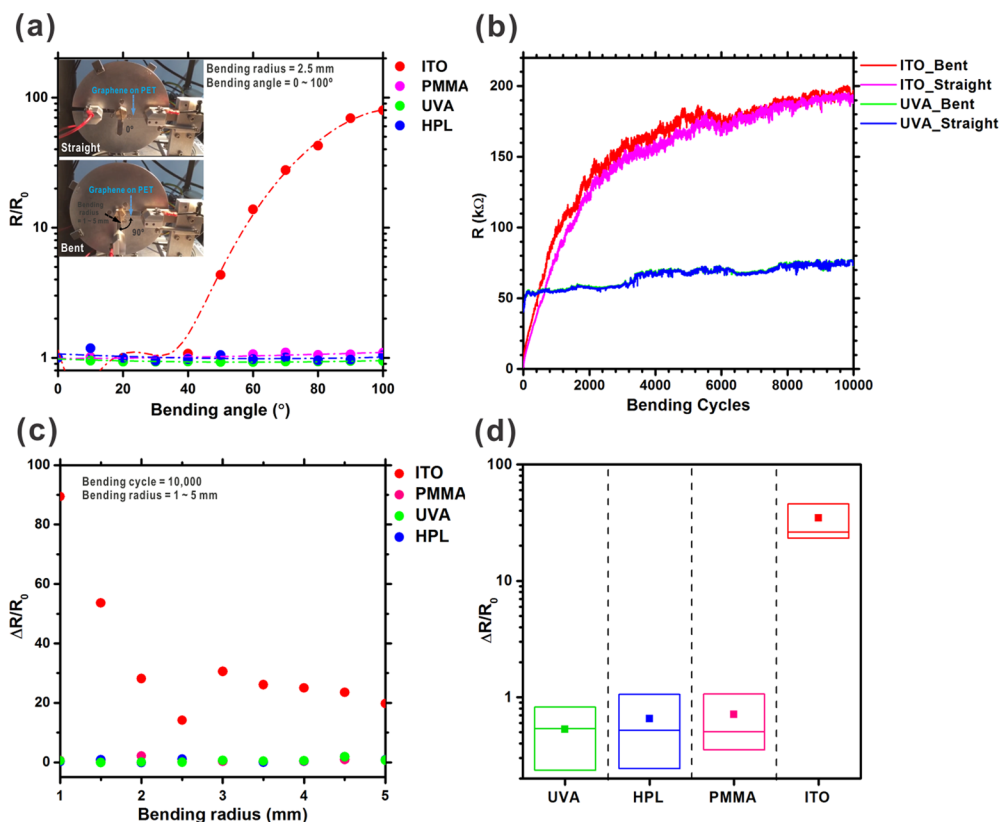
Figure 4. (a) Variation in normalized resistance (R/R_0) as a function of bend angle; inset is the photograph of our custom-built bend rig captured in a bent and relaxed state. (b) Resistance variation of ITO and UVA-graphene as a function of bend cycle, (c) variation of resistance change $(\Delta R/R_0)$ as a function of bend radius for ITO and graphene, and (d) mean $\Delta R/R_0$ for all bending diameters for graphene transferred by UVA, HPL, and PMMA as well as ITO.

stress−strain conditions, as noted by the comparably low electrical resistance of the UVA and HPL methods, even at bending angles of up to 100°. The limited flexibility, with maintained conductivity, of transparent electrodes is considered by many to be the single most significant obstacle facing flexible electronics. The present approach offers one viable solution, though the issue of bending fatigue remains nonetheless critical for most real-world flexible devices.

To assess the bending fatigue performance of the transferred graphene as a function of transfer method, graphene and ITO specimens were bent and relaxed over 10^4 cycles and the differential resistance extracted after each bent and relaxed cycle. Figure 4b shows the measured resistance of ITO and UVA-graphene at 1 mm R_b as a function of bending cycle. The resistance of ITO showed a 95-fold increase from 2 to 190 kΩ after 10^4 cycles with a significant difference in resistance between the maximally bent and straight states. The graphene increased from 46 to 74 kΩ across with the resistance values in the bent state being comparable (less than ±0.5 kΩ) to the straight state, for all cycles.

Various bending radii (1−5 mm) were considered, and the resulting normalized resistance increases $(\Delta R/R_0)$ are as shown in Figure 4c. ΔR denotes the increase in resistance following 10^4 bending fatigue cycles, and R_0 is the initial resistance prior to bending. The resistance of the ITO increased dramatically after 10^4 cycles ($\Delta R/R_0 \approx 20$ at $R_b = 5$ mm). The resistance of ITO showed a considerable increase at $R_b < 2.5$ mm ($\Delta R/R_0 \approx 14$ at $R_b = 2.5$ mm, $\Delta R/R_0 \approx 90$ at $R_b = 1$ mm). Conversely, $\Delta R/R_0$ values for the graphene specimens were not only much smaller (PMMA: 0.5−0.9, UVA: 0.5−0.8, and HPL: 0.2−1.2)

than that of ITO but also showed no visible increasing trend with R_b. The mean normalized changes in the differential channel resistance, $<\Delta R/R_0>$, were calculated and are shown in Figure 4d. From the lower $<\Delta R/R_0>$ for the UVA (0.52) and HPL (0.65) compared to that of PMMA (0.71), we conclude that both the UVA and HPL approaches offer a more mechanically robust system against strain fatigue relative to that of the more conventional PMMA approach.

Unlike their bulk counterparts, two-dimensional materials, and particularly those with microcorrugations, have an extra degree of freedom in the Z direction allowing for effective lateral stress dissipation. Another possible explanation for the superior robustness of graphene in the present mechanical studies is that the strong covalent bonds within the graphitic lattice accommodate significant strain prior to failure.[53] As shown in Figure 4d, the average $\Delta R/R_0$ of UVA and HPL graphene were lower (0.53 and 0.65, respectively) than in the PMMA graphene case (0.71), which are consistent with our earlier bend-angle tests. UVA and HPL graphene do indeed afford more robust mechanical properties than the more commonly adopted PMMA transfer, principally attributed to the higher degree of adhesion between the graphene and substrate. The underpinning mechanisms behind the observed increase in R/R_0 following our fatigue tests was investigated by measuring the surface topology of the bent regions at the specimen centers (for $R_b = 4$ mm) (Agilent AFM 5500). Figure 5a highlights microcrack formation induced by repeated tensile stress in the ITO/PET. The distance between the cracks was around 18 μm, and the crack width was ~40 nm. No such microcracks were noted in any of the graphene samples (Figure 5b−d), with the observed change in R/R_0 in
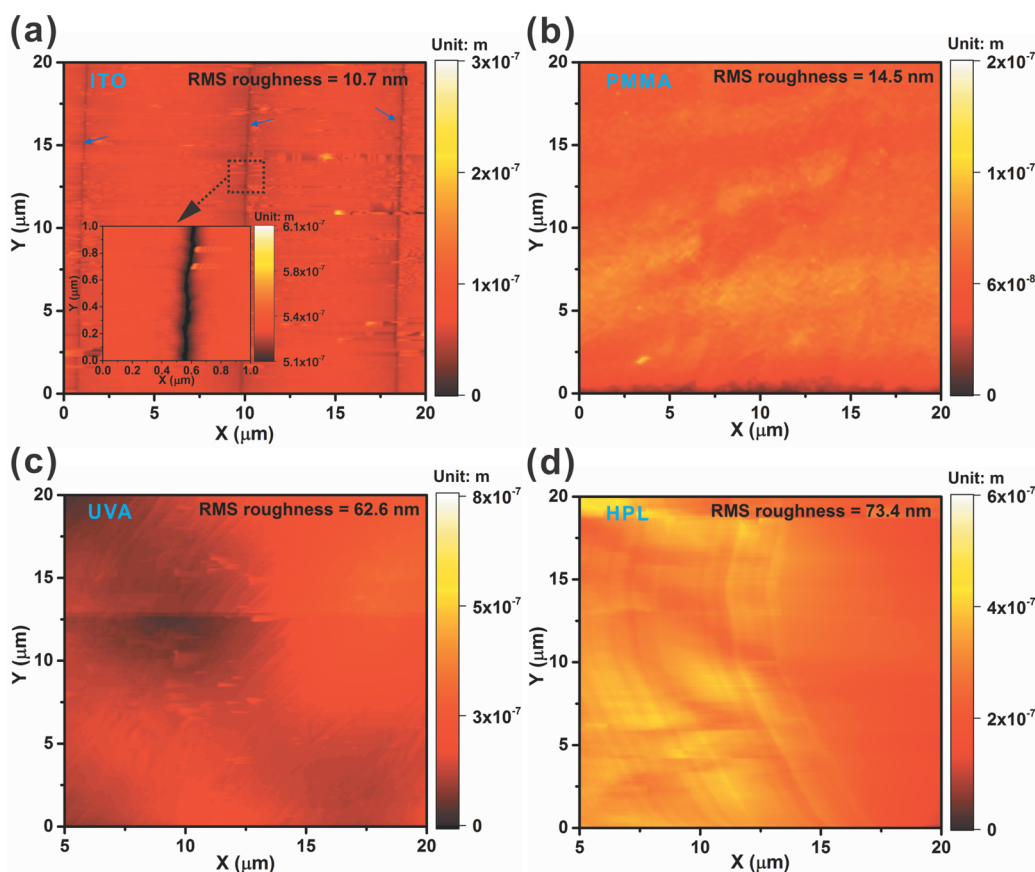
Figure 5. AFM maps of (a) ITO, (b) PMMA-transferred graphene, (c) UVA-transferred graphene, and (d) HPL-transferred graphene on PET after 10^4 bending cycles.

these samples likely attributed to grain movement and to weakened substrate adhesion during repeated bending. As discussed previously, mechanically flexed graphene likely experiences significant defect propagation in the guise of interstitials or vacancy migration which underpin, to a certain extent, microscale intergranular movement, especially if there is compromised or otherwise weakened adhesion to the carrier substrate. In the present geometry and associated stress-concentration mediated therein, such defects likely nucleate further microcracks whose formation and growth are further increased in the presence of reduced interfacial adhesion. Even though repeated bending did not substantially decrease the adhesion between graphene and its substrate, it nonetheless interacted in the first few mechanical fatiguing cycles resulting in a small and irreversible increase in the resistance due to a defect nucleation phase. Such defect growth was clearly passivated in the strain window considered following these few initial cycles. We attribute this to the formation of an equilibrated strain distribution following the initial seasoning strain cycles. The transferred graphene is, in this respect, rather different from ITO, which fails to establish such an equilibrium and continues to electrically degrade with further strain cycling. It is probable that percolative networking effects and associated transport play a central role in the graphene systems ability to resist repeated strain cycles compared to ITO alternatives

a measurable improvement in the mechanical properties relative to conventional PMMA graphene transfer, which we attribute to enhanced adhesion at the substrate—graphene interface. Graphene transferred with the two proposed methods showed lower surface energy and higher degree of adhesion (UVA: 4.40 ± 1.09 N/m, HPL: 0.60 ± 0.26 N/m) compared to equivalent CVD-graphene transferred using conventional PMMA method (0.44 ± 0.06 N/m). Through our bending experiments, we have shown that graphene on PET is more stable under bending stress and is more resistant to microcrack formation than ITO with little variation in normalized resistance for more than 10^4 bend—relax cycles making polymer-supported large-area graphene a compelling platform for the realization of next generation flexible electronics, e-paper, and wearable sensors.

AUTHOR INFORMATION

Corresponding Authors
*E-mail: mhk29@cam.ac.uk.
*E-mail: mtc35@cam.ac.uk.

Notes
The authors declare no competing financial interest.

CONCLUSIONS

Here we have reported on two novel techniques for the transfer of CVD graphene onto flexible and transparent polymeric substrates via UV adhesive (UVA) and hot-press lamination (HPL). These large-area-compatible transfer techniques afforded

■ REFERENCES

(1) Novoselov, K. S.; Geim, A. K.; Morozov, S. V.; Jiang, D.; Zhang, Y.; Dubonos, S. V.; Grigorieva, I. V.; Firsov, A. A. Electric Field Effect in Atomically Thin Carbon Films. *Science* **2004**, *306* (5696), 666−669.

(2) Zhang, Y.; Tan, Y. W.; Stormer, H. L.; Kim, P. Experimental Observation of the Quantum Hall Effect and Berry's Phase in Graphene. *Nature* **2005**, *438* (7065), 201−204.

(3) Han, T.-H.; Lee, Y.; Choi, M.-R.; Woo, S.-H.; Bae, S.-H.; Hong, B. Y.; Ahn, J.-H.; Lee, T.-W. Extremely Efficient Flexible Organic Light-Emitting Diodes with Modified Graphene Anode. *Nat. Photonics* **2012**, *6* (2), 105−110.

(4) Kim, S.-Y.; Kim, J.-J. Outcoupling Efficiency of Organic Light Emitting Diodes Employing Graphene as the Anode. *Org. Electron.* **2012**, *13* (6), 1081−1085.

(5) Wu, J.; Agrawal, M.; Becerril, H. A.; Bao, Z.; Liu, Z.; Chen, Y.; Peumans, P. Organic Light-Emitting Diodes on Solution-Processed Graphene Transparent Electrodes. *ACS Nano* **2010**, *4* (1), 43−48.

(6) Bae, S.; Kim, H.; Lee, Y.; Xu, X. F.; Park, J.-S.; Zheng, Y.; Balakrishnan, J.; Lei, T.; Ri Kim, H.; Song, Y. I.; Kim, Y.-J.; Kim, K. S.; Ozyilmaz, B.; Ahn, J.-H.; Hong, B. H.; Iijima, S. Roll-to-Roll Production of 30-Inch Graphene Films for Transparent Electrodes. *Nat. Nanotechnol.* **2010**, *5* (8), 574−578.

(7) Lee, J.; Cole, M. T.; Lai, J. C. S.; Nathan, A. An Analysis of Electrode Patterns in Capacitive Touch Screen Panels. *J. Disp. Technol.* **2014**, *10* (5), 362−366.

(8) Kim, J.; Ishihara, M.; Koga, Y.; Tsugawa, K.; Hasegawa, M.; Iijima, S. Low-Temperature Synthesis of Large-Area Graphene-Based Transparent Conductive Films Using Surface Wave Plasma Chemical Vapor Deposition. *Appl. Phys. Lett.* **2011**, *98* (9), 091502.

(9) Lin, P.; Choy, W. C. H.; Zhang, D.; Xie, F.; Xin, J.; Leung, C. W. Semitransparent Organic Solar Cells with Hybrid Monolayer Graphene/Metal Grid as Top Electrodes. *Appl. Phys. Lett.* **2013**, *102* (11), 113303.

(10) Park, H.; Brown, P. R.; Bulovic, V.; Kong, J. Graphene as Transparent Conducting Electrodes in Organic Photovoltaics: Studies in Graphene Morphology, Hole Transporting Layers, and Counter Electrodes. *Nano Lett.* **2012**, *12* (1), 133−140.

(11) Un Jung, Y.; Na, S.-I.; Kim, H.-K.; Jun Kang, S. Organic Photovoltaic Devices with Low Resistance Multilayer Graphene Transparent Electrodes. *J. Vac. Sci. Technol., A* **2012**, *30* (5), 050604.

(12) Jo, J. W.; Lee, J. U.; Jo, W. H. Graphene-Based Electrodes for Flexible Electronics. *Polym. Int.* **2015**, *64* (12), 1676−1684.

(13) Park, S.; Ruoff, R. S. Chemical Methods for the Production of Graphenes. *Nat. Nanotechnol.* **2009**, *4* (4), 217−224.

(14) Wu, Y.; Hao, Y.; Jeong, H. Y.; Lee, Z.; Chen, S.; Jiang, W.; Wu, Q.; Piner, R. D.; Kang, J.; Ruoff, R. S. Crystal Structure Evolution of Individual Graphene Islands During Cvd Growth on Copper Foil. *Adv. Mater.* **2013**, *25* (46), 6744−6751.

(15) Torrisi, F.; Hasan, T.; Wu, W.; Sun, Z.; Lombardo, A.; Kulmala, T. S.; Hsieh, G.-W.; Jung, S. M.; Bonaccorso, F.; Paul, P. J.; Chu, D. P.; Ferrari, A. C. Inkjet-Printed Graphene Electronics. *ACS Nano* **2012**, *6* (4), 2992−3006.

(16) Xu, K.; Cao, P.; Heath, J. R. Scanning Tunneling Microscopy Characterization of the Electrical Properties of Wrinkles in Exfoliated Graphene Monolayers. *Nano Lett.* **2009**, *9* (12), 4446−4451.

(17) Kang, J.; Shin, D.; Bae, S.; Hong, B. H. Graphene Transfer: Key for Applications. *Nanoscale* **2012**, *4* (18), 5527−5537.

(18) Li, X.; Cai, W.; An, J.; Kim, S.; Nah, J.; Yang, D.; Piner, R.; Velamakanni, A.; Jung, I.; Tutuc, E.; Banerjee, S. K.; Colombo, L.; Ruoff, R. S. Large-Area Synthesis of High-Quality and Uniform Graphene Films on Copper Foils. *Science* **2009**, *324* (5932), 1312−1314.

(19) Kim, K. S.; Zhao, Y.; Jang, H.; Lee, S. Y.; Kim, J. M.; Kim, K. S.; Ahn, J. H.; Kim, P.; Choi, J. Y.; Hong, B. H. Large-Scale Pattern Growth of Graphene Films for Stretchable Transparent Electrodes. *Nature* **2009**, *457* (7230), 706−710.

(20) Suk, J. W.; Kitt, A.; Magnuson, C. W.; Hao, Y.; Ahmed, S. A.; An, J.; Swan, A. K.; Goldberg, B. B.; Ruoff, R. S. Transfer of Cvd-Grown Monolayer Graphene onto Arbitrary Substrates. *ACS Nano* **2011**, *5* (9), 6916−6924.

(21) Hallam, T.; Wirtz, C.; Duesberg, G. S. Polymer-Assisted Transfer Printing of Graphene Composite Films. *Phys. Status Solidi B* **2013**, *250* (12), 2668−2671.

(22) Zhou, H.; Yu, W. J.; Liu, L.; Cheng, R.; Chen, Y.; Huang, X.; Liu, Y.; Wang, Y.; Huang, Y.; Duan, X. Chemical Vapour Deposition Growth of Large Single Crystals of Monolayer and Bilayer Graphene. *Nat. Commun.* **2013**, *4*, 2096.

(23) Yao, Y.; Wong, C.-P. Monolayer Graphene Growth Using Additional Etching Process in Atmospheric Pressure Chemical Vapor Deposition. *Carbon* **2012**, *50* (14), 5203−5209.

(24) de la Rosa, C. J. L.; Sun, J.; Lindvall, N.; Cole, M. T.; Nam, Y.; Löffler, M.; Olsson, E.; Teo, K. B. K.; Yurgens, A. Frame Assisted H2o Electrolysis Induced H2 Bubbling Transfer of Large Area Graphene Grown by Chemical Vapor Deposition on Cu. *Appl. Phys. Lett.* **2013**, *102* (2), 022101.

(25) Celebi, K.; Cole, M. T.; Teo, K. B.; Park, H. G. Observations of Early Stage Graphene Growth on Copper. *Electrochem. Solid-State Lett.* **2012**, *15* (1), K1−K4.

(26) Sun, J.; Lindvall, N.; Cole, M. T.; Teo, K. B. K.; Yurgens, A. Large-Area Uniform Graphene-Like Thin Films Grown by Chemical Vapor Deposition Directly on Silicon Nitride. *Appl. Phys. Lett.* **2011**, *98* (25), 252107.

(27) Celebi, K.; Cole, M. T.; Choi, J. W.; Wyczisk, F.; Legagneux, P.; Rupesinghe, N.; Robertson, J.; Teo, K. B.; Park, H. G. Evolutionary Kinetics of Graphene Formation on Copper. *Nano Lett.* **2013**, *13* (3), 967−974.

(28) Amini, S.; Garay, J.; Liu, G.; Balandin, A. A.; Abbaschian, R. Growth of Large-Area Graphene Films from Metal-Carbon Melts. *J. Appl. Phys.* **2010**, *108* (9), 094321.

(29) Yoon, D.; Son, Y.-W.; Cheong, H. Negative Thermal Expansion Coefficient of Graphene Measured by Raman Spectroscopy. *Nano Lett.* **2011**, *11* (8), 3227−3231.

(30) Spiecker, E.; Schmid, A. K.; Minor, A. M.; Dahmen, U.; Hollensteiner, S.; Jager, W. Self-Assembled Nanofold Network Formation on Layered Crystal Surfaces During Metal Intercalation. *Phys. Rev. Lett.* **2006**, *96* (8), 086401.

(31) Milne, W. I.; Cole, M. T.; Kang, M. H. Doping Stability and Opto-Electronic Performance of Chemical Vapour Deposited Graphene on Transparent Flexible Substrates. *IET Cir. Dev. & Sys.* **2015**, *9* (1), 39−45.

(32) Martins, L. G.; Song, Y.; Zeng, T.; Dresselhaus, M. S.; Kong, J.; Araujo, P. T. Direct Transfer of Graphene onto Flexible Substrates. *Proc. Natl. Acad. Sci. U. S. A.* **2013**, *110* (44), 17762−7.

(33) Lee, C.; Wei, X.; Kysar, J. W.; Hone, J. Measurement of the Elastic Properties and Intrinsic Strength of Monolayer Graphene. *Science* **2008**, *321* (5887), 385−388.

(34) Wei, N.; Xu, L.; Wang, H.-Q.; Zheng, J.-C. Strain Engineering of Thermal Conductivity in Graphene Sheets and Nanoribbons: A Demonstration of Magic Flexibility. *Nanotechnology* **2011**, *22* (10), 105705.

(35) Ni Annaidh, A.; Bruyere, K.; Destrade, M.; Gilchrist, M. D.; Ottenio, M. Characterization of the Anisotropic Mechanical Properties of Excised Human Skin. *J. Mech. or Bio. Mater.* **2012**, *5* (1), 139−48.

(36) Pourzand, H.; Tabib-Azar, M. Graphene Thickness Dependent Adhesion Force and Its Correlation to Surface Roughness. *Appl. Phys. Lett.* **2014**, *104* (17), 171603.

(37) Shin, Y. J.; Wang, Y.; Huang, H.; Kalon, G.; Wee, A. T.; Shen, Z.; Bhatia, C. S.; Yang, H. Surface-Energy Engineering of Graphene. *Langmuir* **2010**, *26* (6), 3798−802.

(38) Gao, W.; Huang, R. Effect of Surface Roughness on Adhesion of Graphene Membranes. *J. Phys. D: Appl. Phys.* **2011**, *44* (45), 452001.

(39) Rafiee, J.; Mi, X.; Gullapalli, H.; Thomas, A. V.; Yavari, F.; Shi, Y.; Ajayan, P. M.; Koratkar, N. A. Wetting Transparency of Graphene. *Nat. Mater.* **2012**, *11* (3), 217−22.

(40) Raj, R.; Maroo, S. C.; Wang, E. N. Wettability of Graphene. *Nano Lett.* **2013**, *13* (4), 1509−15.

(41) Packham, D. E. Work of Adhesion: Contact Angles and Contact Mechanics. *Int. J. Adhes. Adhes.* **1996**, *16*, 121−128.

(42) Nakamura, Y.; Kamada, K.; Katoh, Y.; Watanabe, A. Studies on Secondary Electrocapillary Effects: 1. Confirmation of Young-Dupre Equation. *J. Colloid Interface Sci.* **1973**, *44* (3), 517−524.

(43) Owens, D. K.; Wendt, R. C. Estimation of Surface Free Eenergy of Polymers. *J. Appl. Polym. Sci.* **1969**, *13* (8), 1741.

(44) Moutinho, I.; Figueiredo, M.; Ferreira, P. Evaluating the Surface Energy of Laboratory-Made Paper Sheets by Contact Angle Measurements. *Tappi J.* **2007**, *6* (6), 26−32.

(45) Bradley, R. S. The Cohesive Force between Solid Surfaces and the Surface Energy of Solids. *Philos. Mag.* **1932**, *13* (86), 853−862.

(46) Medendrop, C. A. Antomic Force Microscopy Method Development for Surface Energy Analysis. Doctoral dissertation, University of Kentucky, Lexington, KY, 2011.

(47) Hejda, F.; Solǎr, P.; Kousal, J. Surface Free Energy Determination by Contact Angle Measurements. In *WDS'10 Proceedings of Contributed Papers*; Safrankova, J., Pavlu, J., Eds.; Matfyzpress: Prague, 2010; Part *II*, pp 25−30.

(48) Barthel, E. Adhesive Elastic Contacts: Jkr and More. *J. Phys. D: Appl. Phys.* **2008**, *41* (16), 163001.

(49) Prieto-López, L. O.; Williams, J. A. Using Microfluidics to Control Soft Adhesion. *J. Adhes. Sci. Technol.* **2016**, *30* (14), 1555−1573.

(50) Lee, S.-M.; Kim, J.-H.; Ahn, J.-H. Graphene as a Flexible Electronic Material: Mechanical Limitations by Defect Formation and Efforts to Overcome. *Mater. Today* **2015**, *18* (6), 336−344.

(51) Lacombe, R. Applied Adhesion Testing. In *Adhesion Measurement Methods*; CRC Press: Boca Raton, FL, 2005; pp 187−248.

(52) Koenig, S. P.; Boddeti, N. G.; Dunn, M. L.; Bunch, J. S. Ultrastrong Adhesion of Graphene Membranes. *Nat. Nanotechnol.* **2011**, *6* (9), 543−546.

(53) Galiotis, C.; Tsoukleri, G.; Frank, O.; Parthenios, J.; Papagelis, K.; Novoselov, K. S. Mechanical Properties of Graphenes and Graphene Polymer Nanocomposites. In *ECCM15−Proceedings of the 15th European Conference on Composite Materials*, Venice, Italy, June 24−28, 2012.